Lab on a Chip

PAPER

Scalable production of double emulsion drops with thin shells

A. Vian, B. Reuse and E. Amstad*

Received 00th January 20xx,
Accepted 00th January 20xx

DOI: 10.1039/x0xx00000x

www.rsc.org/

Double emulsions are often used as containers to perform high throughput screening assays and as templates for capsules. These applications require double emulsions to be mechanically stable such that they do not coalesce during processing and storage. A possibility to increase their stability is to reduce the thickness of their shells to sufficiently low values that lubrication effects hinder coalescence. However, the controlled fabrication of double emulsions with such thin shells is difficult. Here, we introduce a new microfluidic device, the aspiration device, that reduces the shell thickness of double emulsions down to 240 nm at a high throughput; thereby, the shell volume is reduced by up to 95%. The shell thickness of the resulting double emulsions depends on the pressure profile in the device and hence on the fluid flow rates in the channels and is independent of the shell thickness of the injected double emulsions. Therefore, this device enables converting double emulsions with polydisperse shell thicknesses into double emulsions with well-defined, uniform thin shells.

Introduction

Emulsion drops are often used as picoliter-sized vessels to conduct chemical[1,2] and biochemical reactions,[3,4] and for high throughput screening assays.[5–7] These drops can be produced at high frequencies allowing compartmentalization of large quantities of reagents in a short amount of time.[8-10] To take advantage of the possibility to produce large quantities of samples in a minimum amount of time, they must be analyzed at high rates. A fast read-out technique that is routinely used in biology is fluorescence activated cell sorting (FACS).[11-15] However, this technique has thus far only been applied for characterizing analytes that are dispersed in aqueous solutions, such as cells.[16] This requirement is not limiting if colonies of cells are analyzed because they are typically dispersed in aqueous solutions. By contrast, many drops encompassing analytes, such as reagents, proteins, or individual cells, are aqueous such that they are dispersed in an oil that has a low solubility in water. To sort aqueous drops containing reagents using FACS, they have been loaded into water-oil-water double emulsion drops, which are aqueous drops contained in larger oil-based drops that are dispersed in an aqueous surrounding.[5,6,14-17] For these assays to be truly useful, double emulsions must be stable against coalescence. The mechanical stability of double emulsions increases with decreasing shell thickness: The hydrodynamic resistance increases with decreasing shell thickness, thereby hampering the oil flow inside the shell and introducing lubrication effects.[18] The impeded oil flow in the shell retards the motion of the innermost aqueous drop relative to the outer oil drop, thereby delaying or even preventing the innermost aqueous drop from merging with the continuous aqueous phase.[19,20] As a result of this lubrication effect, local variations in thickness of the double emulsion shells decrease with decreasing shell thickness.[21]

Double emulsions with controlled shell thicknesses can be assembled using microfluidics.[21-23] These drops usually have shells with thicknesses ranging from a few µm up to several tens of µm. Double emulsions with much thinner shells, below 1 µm, can be produced from microfluidic glass capillary devices.[24-30] However, the fabrication of these devices is tedious. Moreover, they often produce mixtures of single and double emulsion drops that must be separated after they have been produced. To facilitate the production of double emulsions with thin shells, microfluidic devices made of poly(dimethyl siloxane) (PDMS) have been developed.[31] These devices produce double emulsions with shell thicknesses down to 4 µm. Their shell thickness can be reduced if double emulsions are pushed through constrictions.[32,33] However, this reduction in the shell thickness is only controlled and reproducible if one double emulsion passes the constriction at a time; this requirement limits the throughput of these devices. Devices that reduce the shell thickness of double emulsions below 1 µm at a rate similar or even exceeding their production rate remain to be established. These devices would facilitate the use of double emulsions for high throughput screening assays and open up new possibilities to employ them as templates to produce capsules with well-defined thin shells.

In this paper, we report a microfluidic device, the aspiration device, that reduces the thickness of water-oil-water double emulsion shells down to 240 nm at a rate similar to the typical

Soft Materials Laboratory, Institute of Materials, École Polytechnique Fédérale de Lausanne, 1015 Lausanne, Switzerland. E-mail: esther.amstad@epfl.ch

Electronic Supplementary Information (ESI) available: High-speed camera movies showing double emulsion drops passing through the aspiration device at different flow rates.

production rate of double emulsions in flow focusing devices. This is achieved by injecting primary water-oil-water double emulsions with thick shells into the main microfluidic channel. The main channel is intersected by many much smaller shunt channels that remove up to 95 vol% of the oil contained in the double emulsion shells. This new microfluidic aspiration device allows processing hundreds of double emulsions at the time. Thereby, it offers possibilities to produce double emulsions with thin shells at throughputs that are at least an order of magnitude higher than what could previously been achieved media.

Experimental section

Device fabrication

We fabricate the microfluidic aspiration device from poly(dimethyl siloxane) (PDMS) using soft lithography.[34,35] It consists of a main channel that is 80 µm tall and 60 µm wide and guides the drops through the aspiration section. Within the aspiration section, each of two oppositely positioned sides of the main channels is intersected by n = 30 parallel shunt channels with cross sections of 10 µm × 20 µm. Each of these shunt channels leads into one of two large aspiration reservoirs that are connected to a single outlet. The surfaces of the shunt channels are treated to be wetting to the middle phase. To reduce the shell thickness of water-oil-water double emulsions, where the oil is perfluorinated, we treat the channels with a HFE7500-based solution containing 1 vol% perfluorinated trichlorosilane. To reduce the shell thickness of water-oil-water double emulsions where the oil is hydrocarbon-based, we refrain from any surface modification because the PDMS surface is hydrophobic.

Production of water-oil-water double emulsions

Water-oil-water double emulsion drops with shell thicknesses ranging from 4 to 15 µm are formed using PDMS-based microfluidic devices.[32] As an innermost phase, we employ an aqueous solution containing 20 wt% poly(ethylene glycol) (PEG, M_w = 6 kDa); PEG is added to increase the viscosity of the inner phase, thereby facilitating the assembly of double emulsion drops. The middle phase is composed of a perfluorinated oil, HFE7500, containing 1 wt% of a triblock surfactant that has two perfluorinated blocks that are separated by a PEG-based block.[36,37] The outermost aqueous phase contains 10 wt% partially hydrolyzed poly(vinyl alcohol) (PVA) (M_w = 13-23 kDa).

Operation of the aspiration device

The aspiration device removes oil contained in water-oil-water double emulsions most efficiently, if they are injected at a high density such that they jam inside the main channel. To increase the density of double emulsions, we up-concentrate them by letting them sediment or cream for at least 10 min before a fraction of the surrounding aqueous phase is removed. The up-concentrated double emulsions are introduced into the aspiration device using syringe pumps at an injection rate Q_i. To tune the amount of oil that is removed through the shunt channels we withdraw fluid through two aspiration reservoirs that are connected to an outlet at a withdraw rate Q_w. The vast majority of the surrounding aqueous phase that initially separates adjacent double emulsions is removed through the shunt channels such that the double emulsions are jammed within the main channel. To increase the spacing between adjacent drops after they passed all the shunt channels, we introduce a flow-focusing junction downstream the aspiration section and inject the outermost phase at a rate Q_o. The resulting double emulsion drops with thin shells are collected through a second outlet.

To quantify the shell thicknesses of double emulsions, we measure the outer radius of the intact double emulsions from optical micrographs. The double emulsions are subsequently broken using isopropanol and the size of the resulting single emulsion oil drop is measured from optical microscopy images. Using volume conservation, we calculate the shell thickness from the radius of the intact double emulsion drop and the volume of the oil drop that forms after the double emulsion is broken, as previously reported[19,25,33,38] and detailed in the Supporting Information. To test the accuracy of this quantification method, we employed this technique to measure the dimensions of double emulsions with thick shells and compared it to values optained from optical microscopy and from the known injection rates of the different fluids and the drop generation frequency using mass conservation, as detailed in the supporting information.[33]

Quantification of the velocity profile of drops in the aspiration section

To quantify the velocity of drops in the aspiration section as a function of their location, we acquire optical microscopy

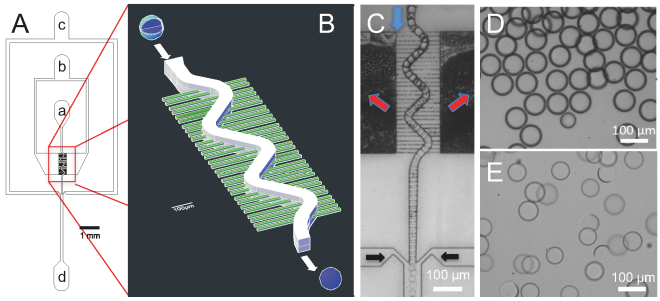

Fig. 1: The microfluidic aspiration device. (A) Schematic illustration of the microfluidic aspiration device that contains an inlet for double emulsions drops (a), an outlet that enables withdrawing oil from the double emulsions (b), and an inlet for the outermost aqueous solution (c). Processed double emulsions are collected through outlet (d). (B) 3D schematic illustration of the aspiration section where the shell thickness of double emulsions is reduced, as schematically illustrated with double emulsions containing an aqueous core (blue) and an oil shell (light blue). The aspiration section contains a main channel (white) that is intersected by many much smaller shunt channels (green). (C) Optical microscopy image of the aspiration device in operation. The double emulsion drops flow through a sinoidal shaped main channel, as indicated by the blue arrow, and oil is removed through shunt channels as indicated by the red arrows. To increase the spacing between processed double emulsions, an outermost aqueous phase is injected downstream the aspiration section, as shown by the black arrows. (D, E) Optical micrographs of double emulsions drops (D) before and (E) after being processed with the aspiration device. Double emulsions have an external radius of (D) R = 42.9 ± 0.5 µm and (E) R = 36.0 ± 0.6 µm and a shell thickness of (D) d = 5.92 ± 0.64 µm and (E) d = 0.24 ± 0.05 µm.

images using a high speed camera, Phantom V7, operated at a 3000 frames per second (fps), as detailed in the supporting information.

Quantification of the viscosity

The viscosities of the oils are quantified with a DHR3 Rheometer using the coaxial cylinder geometry (TA Instrument). We vary the shear rate from 0.1 to 100 s^{-1}, keeping the strain constant at 1%.

Results and discussions

We fabricate the PDMS-based microfluidic aspiration device using soft lithography.[34,35] It contains an inlet for as-produced primary double emulsions, inlet a, that leads into a main channel, as shown schematically in Figure 1A. The double emulsions flow through the aspiration section where two opposite sides of the main channel are intersected by shunt channels; unless stated otherwise, each of these sides is intersected by n = 30 shunt channels, as schematically illustrated in Figure 1B and shown on the optical micrograph in Figure 1C. The main channel has a sinusoidal shape to increase its contact area with the shunt channels. These shunt channels lead into one of two aspiration reservoirs that are both connected to outlet b, as shown in Figure 1A. To control the spacing of the processed double emulsions with thin shells, we introduce a flow focusing junction downstream the aspiration unit, as indicated by the black arrows in Figure 1C and in movie S1.

Water-oil-water double emulsions with an external radius of R = 42.9 ± 0.5 µm and a shell thickness of d = 5.92 ± 0.64 µm are produced using PDMS-based flow focusing devices.[34,35] To reduce the thickness of their oil shells, we inject them into the aspiration device at a rate Q_i = 1000 µL/h, as shown by the blue arrow in Figure 1C. Oil is removed through the shunt channels at a withdraw rate, Q_w = 900 µL/h, as indicated by the red arrows in Figure 1C. While the drops pass the initial parts of the aspiration section, a large fraction of the surrounding aqueous phase flows through the shunt channel into outlet b such that the distance between adjacent drops gradually decreases until they start to jam. To spatially separate the processed double emulsions with thin shells, we introduce a flow focusing junction downstream the aspiration section through which we inject an aqueous outer solution at a rate Q_o = 800 µL/h, as indicated by the black arrows in Figure 1C. The resulting double emulsions have much thinner shells, as a comparison of the optical micrographs of double emulsions before and after they have been processed with the aspiration device in Figures 1D and 1E reveals. Indeed, the shell thickness of double emulsions that have been processed with the aspiration device is reduced from d = 5.92 ± 0.64 µm to 0.24 ± 0.05 µm. As a result of the reduction in shell thickness, the radius of the processed double emulsion is slightly reduced to R = 36.0 ± 0.6 µm.

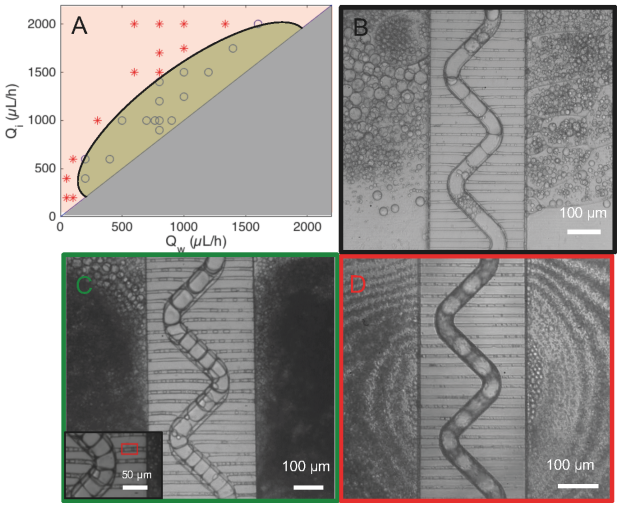

Fig. 2: Operation of the aspiration device. (A) Influence of the injection rate, $\boldsymbol{Q_i}$ and the withdraw rate, $\boldsymbol{Q_w}$, on the operation of the device. Operation conditions that result in double emulsions with a standard deviation of the shell thickness $\sigma \geq 0.1$ µm (o), and $\sigma \leq 0.1$ µm (∗). If $\boldsymbol{Q_w} > \boldsymbol{Q_i}$, the vast majority of double emulsions exit the device through the shunt channel such that we cannot control their shell thickness; this regime is indicated in grey. Based on the results, we indicate the optimum operation conditions in green and conditions where the device fails to consistently remove oil in red. (B-D) Optical micrographs of the aspiration device operating (B) in the grey area where the majority of double emulsions exit the device through the shunt channels, (C) under optimal conditions, and (D) when it fails.

The operation mode of microfluidic devices typically depends on the fluid flow rates. To explore the different operation modes of the aspiration device, we vary the withdraw and injection rates from 50 µL/h to 2000 µL/h. If the withdraw rate is higher than the injection rate, $Q_w > Q_i$, the vast majority of fluids, including the double emulsion drops, are aspirated through the shunt channels such that very few double emulsions exit the main channel, as indicated by the grey area in Figure 2A and the optical micrograph in Figure 2B. Instead, much smaller double emulsions, whose diameter is of order of the width of the shunt channels are formed at their exits, as shown in movie S2. This operation resembles the extrusion used, for example, to process vesicles[39] and can be employed to reduce the size of double emulsions. However, this operation mode does not offer a good control over the shell thickness of double emulsions such that we do not further investigate it here. By contrast, if the injection rate is higher than the withdraw rate, $Q_i > Q_w$, double emulsions remain intact. Hence, if $Q_i > Q_w$, we can reduce the shell thickness of double emulsions without significantly altering their diameter.

To control the spacing of the processed double emulsions, we introduce a flow focusing junction downstream the aspiration section and inject an aqueous phase containing a surfactant, PVA, through it. We assume this additional fluid not to impact the operation of the device and the final shell thickness of double emulsions because the width of the main channel increases three-fold at the flow focusing junction. Hence, the hydrodynamic resistance of the channel downstream the aspiration section is more than five-fold lower than that of the aspiration section, as demonstrated in the supporting information. To verify this assumption, we vary Q_o from 300 to 6000 µL/h, keeping Q_i and Q_w constant. Within the tested flow rate range, Q_o does not significantly influence the double emulsion shell thickness: Varying Q_o by a factor of 20 results in shell thickness variations of less than 10%, as shown in Figure S1. Therefore, we keep Q_o constant at 800 µL/h for all the remaining experiments and do not further investigate this parameter.

The dimensions of double emulsion drops generated in microfluidic flow focusing devices depend on the fluid flow

rates. To test if this is also the case for the aspiration device, we vary the injection and withdraw rates for $Q_i > Q_w$. We consider the aspiration device to function properly, if the standard deviation of the shell thickness, σ, is below 0.1 µm. This is the case if double emulsions are injected at rates exceeding the withdraw rates by more than 50% and if $Q_i >$ 250 µL/h, as summarized by the green shaded area in Figure 2A and shown in the optical micrograph in Figure 2C. By contrast, if $Q_i <$ 250 µL/h or if $Q_i > 0.5Q_w$, the shell thicknesses of the processed double emulsions are polydisperse, as summarized by the red shaded area in Figure 2A and in the optical micrograph in Figure 2D. We assign this behavior to the pressure profile in the device: The pressure in the main channel within the aspiration section decreases because a significant fraction of the liquid is removed through the shunt channels.[4] As a result, the pressure difference between the main channel and the aspiration reservoir, and therefore the pressure gradient across the shunt channels, gradually decreases within the aspiration section, as detailed in the supporting information. With decreasing pressure gradient across the shunt channels, the driving force for oil to be removed from the double emulsion shells is reduced. At some point, the pressure gradient is so small that no oil is removed any more. In fact, if the ratio of the withdraw to the injection rate is too low, the pressure gradient in the shunt channels located towards the end of the aspiration section becomes negative such that some of the oil contained in the reservoir is re-injected into the main channel, as shown in the optical micrograph in Figure 2D and movie S3. This re-injected oil broadens the distribution of the shell thicknesses of the processed double emulsions. Based on these results, the remaining experiments are conducted in the green shaded area.

The dimensions of emulsions produced in microfluidic devices can often be tuned with the fluid flow rates. To test if this is also the case for the aspiration device, we vary Q_i from 1600 µL/h to 900 µL/h h and keep Q_w constant at 800 µL/h. The shell thickness linearly decrease with decreasing Q_i, as shown by the red diamonds in Figure 3A. Similarly, if we decrease Q_w from 800 µL/h to 200 µL/h and keep Q_i constant at 900 µL/h, the shell thickness linearly increases, as shown by the blue circles in Figure 3A. The excellent agreement of the shell thicknesses obtained by varying either Q_i or Q_w and keeping the other flow rate constant suggests that the shell thickness depends on the difference in Q_i and Q_w, $\Delta Q = Q_i$-Q_w only and does not depend their absolute values. To test this suggestion, we vary the absolute values of Q_i and Q_w, keeping ΔQ constant at 200 µL/h. Indeed, the shell thickness of double emulsions is independent of the absolute values of Q_i and Q_w, as shown in Figure 3B.

Our results suggest that the shell thickness of processed double emulsions is determined by the pressure gradient across the shunt channels and hence, by the pressure profile in the aspiration section. To better understand this result, we estimate the pressure profile across the main channel using an electric circuit analogue, as shown in Figure S2 and detailed in the supporting information. For constant ΔQ, the model predicts the pressure to drop quickly in the first part of the aspiration section and level off thereafter as seen in Figure S3A. Interestingly, while the pressure in the initial parts of the aspiration section depends on Q_i, it varies very little with the absolute value of Q_i at the end of the aspiration section, as shown in Figure S4A. To test the validity and accuracy of the model, we convert the pressure profile into a velocity profile of the drops in the main channel, as detailed in the supporting information, and compare it to experimental results. To experimentally quantify the velocity profile, we monitor the flow of the drops in the aspiration section using a high-speed camera and measure the drop speed as a function of the location within the channel, as exemplified in Figure S5 and detailed in the supporting information. Because liquid is continuously removed through the shunt channels, the speed of the drops in the main channel successively decreases, well in agreement with our model, as a comparison of the symbols and the solid line in Figure 3C reveals. As expected, the initial speed of injected drops increases with increasing Q_i. Our model predicts the speed of the drops in the final parts of the aspiration section to only depend on ΔQ. To test this prediction, we keep ΔQ constant at 300 µL/h and vary Q_i between 1000 µL/h and 2000 µL/h. Indeed, the velocity of the drops at the end of the aspiration section is the same, 18 mm/s, as shown in Figure 3C, well in agreement with our

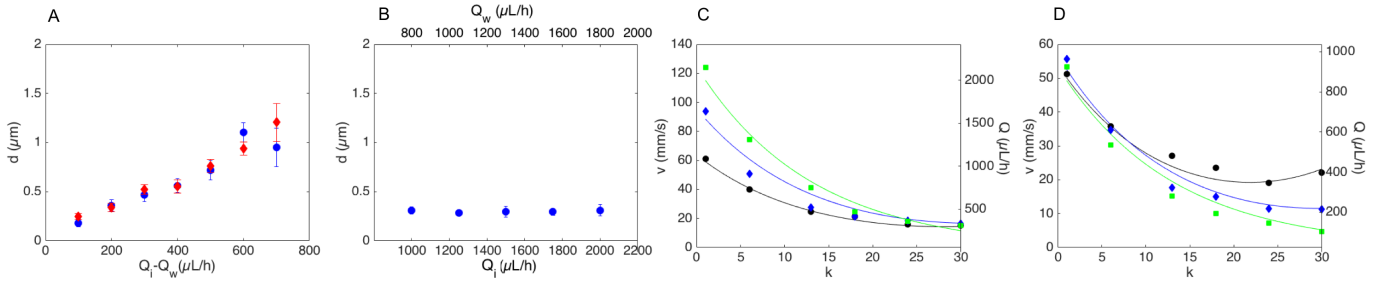

Fig. 3: Influence of fluid flow rates on the shell thickness of processed double emulsions. (A) Influence of the injection rate, $\boldsymbol{Q_i}$, and withdraw rate, $\boldsymbol{Q_w}$, on the thickness of processed double emulsions, $\boldsymbol{d}$ if $\boldsymbol{Q_i}$ is varied and $\boldsymbol{Q_w}$ is kept constant at 800 µL/h (◆) or if $\boldsymbol{Q_w}$ is varied and $\boldsymbol{Q_i}$ is kept constant at 1000 µL/h (●). (B) Influence of $\boldsymbol{Q_i}$ and $\boldsymbol{Q_w}$ on $\boldsymbol{d}$ if $\boldsymbol{\Delta Q}$ is kept constant at 200 µL/h. (C) Velocity of drops, $\boldsymbol{v}$, and corresponding flow rate, $\boldsymbol{Q}$, as a function of their location in the main channel measured as the number of shunt channels located upstream the location of interest, $\boldsymbol{k}$, for $\boldsymbol{\Delta Q}$ = 300 µL/h and $\boldsymbol{Q_i}$ = 1000 µL/h (●), 1500 µL/h (◆) and 2000 µL/h (■). The velocity profile of fluids is estimated using an electric circuit analogue using $\boldsymbol{Q_i}$ = 1000 µL/h (black solid line), 1500 µL/h (blue solid line) and 1000 µL/h (green solid line). (D) Speed profile, $\boldsymbol{v}$, and corresponding fluid flow rate, $\boldsymbol{Q}$, in the main channel as a function of the location in main channel, $\boldsymbol{k}$, for $\boldsymbol{Q_i}$ = 1000 µL/h and $\boldsymbol{\Delta Q}$ = 100 µL/h (■), 200 µL/h (◆) and 400 µL/h (●). The corresponding calculated values are shown by the solid lines.

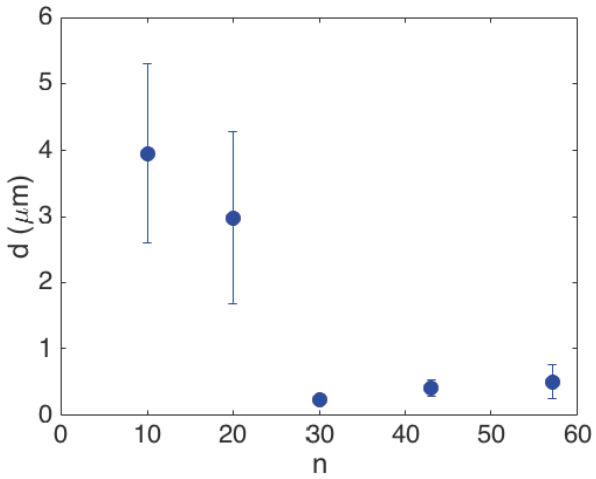

Fig. 4: Influence of the number of shunt channels, $\boldsymbol{n}$, on the shell thickness of processed double emulsions, $\boldsymbol{d}$, that were injected with Q_i = 1000 µL/h, whereas Q_w = 800 µL/h and Q_o = 800 µL/h.

model. To further experimentally test our model prediction, we inject the drops at a constant rate Q_i and vary ΔQ. While the speed of the double emulsions in the initial part of the aspiration section is the same, their velocity in the final section decreases with increasing ΔQ, as shown in Figure 3D. For example, the speed of double emulsions injected with Q_i = 900 µL/h decreases from 53 mm/s to 5 mm/s if ΔQ = 100 µL/h, but decreases only to 12 mm/s if ΔQ = 200 µL/h. These results demonstrate that even though we employ a very simple model that, for example, neglects any contribution of the drops contained in the main channel to its induced hydrodynamic resistance,[40] it correctly captures influences of fluid flow rates on the pressure and velocity profile in the main channel. These parameters are directly related to the shell thickness of processed double emulsions such that we can use this model to optimize the device design and operation conditions.

The velocity of the drops strongly decreases as they pass the first 15 shunt channels and levels off thereafter as seen in Figures 3C and 3D. The non-linear deceleration of drops in the aspiration section suggests that the amount of removed fluid quickly decreases as drops pass the aspiration device. However, it is unclear whether the total amount of removed fluid directly correlates with the amount of oil removed from the double emulsion shells. To decouple the removal of the continuous phase from that of the oil, we fabricate aspiration devices with n = 10, 20, 43 and 57 shunt channels and measure the thickness of double emulsions processed with these devices. Thereby, we keep the injection and withdraw rates constant at Q_i= 1000 µL/h and Q_w= 800 µL/h. Devices with no more than 20 shunt channels fail to efficiently and consistently remove the oil from double emulsion shells: These devices remove a considerable amount of the continuous phase but only a limited amount of the oil. For example, devices with n = 10 shunt channels reduce the shell by only 39 vol% whereas devices with n = 20 shunt channels reduce the shell volume by 54%. This oil removal is much lower than achieved in devices with n = 30 shunt channels where it amounts to 95 vol%, as summarized in Figure 4. We assign the much lower oil removal efficiency obtained in devices with $n \leq 20$ to the density of the drops in the main channel: While these devices remove a considerable amount of the continuous phase, adjacent drops are still spatially separated from each other by the continuous phase such that they do not jam. By contrast, for devices with $n \geq 20$, a sufficient amount of continuous phase is removed such that drops jam. This observation suggests that jamming is crucial for an efficient removal of the oil. In line with this observation, the shell thickness distribution of double emulsions processed in devices with $n \leq 20$ is much broader than if processed in devices with more shunt channels, as shown by the large error bars in Figure 4.

Our results suggest that oil is most efficiently removed if drops are jammed. To test if we can reduce the shell thickness of double emulsions even more, we prolong the time jammed drops are in the aspiration section by increasing the number of shunt channels. If we process double emulsions in devices with n = 43 shunt channels, they have slightly thicker shells than if processed in device with n = 30. Their shell thickness increases even more if n is increased to 57, as shown in Figure 4. These results indicate that there is an optimum number of shunt channels. If this optimum is exceeded, the pressure gradient across the shunt channels located furthest downstream becomes negative such that some of the oil, that initially has been removed from double emulsion shells, is re-injected into them further downstream. For water-oil-water double emulsions composed of a shell with a viscosity of order of that of water, and for ΔQ= 200 µL/h, this optimum is around n = 30.

Our results indicate that the shell thickness of double emulsions processed with the aspiration device depend on the velocity at the end of the channel only. Therefore, we expect it to be independent of the shell thickness of the primary double emulsions. To test this expectation, we produce primary double emulsions with shell thickness varying between d = 2.31 ± 0.22 µm and d = 7.01 ± 0.73 µm. These double emulsions are injected into the aspiration device at Q_i = 1000 µL/h and we withdraw fluids at Q_w = 800 µL/h. Independent of the shell thickness of primary emulsion drops, that of the processed double emulsion drops is d = 0.37 ± 0.11 µm, as shown in Figure 5A. These results suggest that the aspiration device can reduce the distribution of shell thicknesses in double emulsions. To demonstrate this feature, we fabricate a mixture of double emulsions with an external radius of 53.1 ±

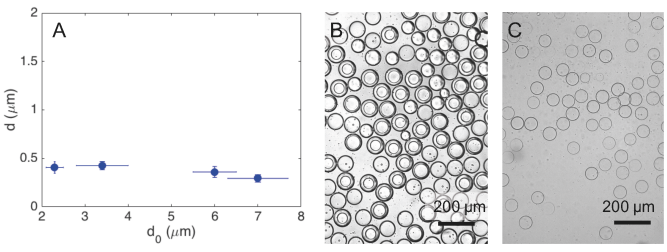

Fig. 5: Influence of the shell thickness of primary double emulsions. (A) Influence of the shell thickness of primary double emulsions, $\boldsymbol{d_0}$, on that of processed counterparts, $\boldsymbol{d}$, for initial double emulsions with $\boldsymbol{d_0}$= 2.3 ± 0.2 µm, 3.4 ± 0.6 µm, 6 ± 0.5 µm and 7 ± 0.7 µm. (B, C) Optical micrographs of (B) primary double emulsions that have polydisperse shell thicknesses with $\boldsymbol{d_0}$ = 10.3 ± 6.2 µm and (C) double emulsions after they have been processed with the aspiration device, whose shell thickness is $\boldsymbol{d}$ = 0.272 ± 0.081 µm.

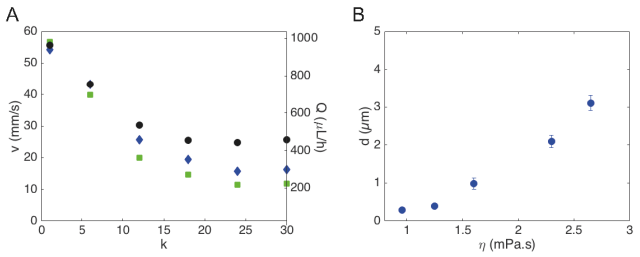

Fig. 6: Influence of the oil viscosity. (A) Velocity of drops, $\boldsymbol{v}$, as a function of the number of shunt channels located further upstream, $\boldsymbol{k}$, of double emulsions with oil shells whose viscosity is η = 0.96 mPa.s (■), 1.25 mPa.s (◆) and 1.6 mPa.s (●). The flow rates are kept constant at Q_i = 1000 µL/h, Q_w = 800 µL/h, and Q_o= 800 µL/h. (B) Influence of the viscosity of the oil, $\boldsymbol{\eta}$, contained in the double emulsion shells on their shell thickness, $\boldsymbol{d}$. Double emulsions have been processed with Q_i = 1000 µL/h, Q_w = 800 µL/h and Q_o = 800 µL/h.

1.8 µm, whose shell thicknesses vary from 5 to 20 µm, as shown in the optical micrograph in Figure 5B. After this mixture has been processed with the aspiration device, we obtain double emulsions whose shell thicknesses vary by as little as 80 nm, as indicated by the narrow distribution of the shell thicknesses of double emulsions shown in Figure 5C. These results demonstrate the potential of the aspiration device to process polydisperse single-core double emulsions into double emulsions with well-defined shell thicknesses and thereby to facilitate the control over their mechanical stability and permeability.

The aspiration device removes up to 95 vol% of the oil from the shell of double emulsions. We expect the fraction of removed oil to depend on the fluid viscosity because this parameter influences the hydrodynamic resistance of the shunt channels and hence the pressure gradient across them. To test this expectation, we vary the viscosity of the oil, η, from 0.9 to 2.7 mPa.s by adding different amounts of Krytox^{TM} GPL, a more viscous perfluorinated oil, to HFE7500.[33] Indeed, the amount of oil that is removed decreases with increasing oil viscosity such that the velocity of the double emulsions at the end of the aspiration section increases, as shown in Figure 6A. As a result, the shell thickness of the processed double emulsion increases with increasing oil viscosity, as shown in Figure 6B.

To demonstrate the versatility of the device, we produce primary water-oil-water double emulsions with different oils. In particular, we employ a hydrocarbon-based oil, oleic acid, and a liquid crystal (4-Cyano-4-n-pentylbiphenyl, Sigma). The aspiration device reduces the volume of double emulsion shells composed of oleic acid by 83% from 4.67 ± 0.29 µm to 0.88 ± 0.21 µm, as illustrated in movie S4. Similarly, the volume of shells composed of a liquid crystal is reduced by 81% from 5.70 ± 0.49 µm to 1.20 ± 0.21 µm, as shown in Figure S6. These results demonstrate that the aspiration device is not limited to the removal of perfluorinated oils but can be employed to remove many other fluids from shells of double emulsions.

Conclusion

We introduce a microfluidic aspiration device that enables reducing the shell volume of up to 1000 double emulsions per second by up to 95 vol%. The resulting double emulsions have shell thicknesses down to 240 nm. Importantly, the oil removal does not rely on a partitioning of the solvent into the continuous phase nor does it involve solvent evaporation. Hence, this device allows reducing the shell thickness of double emulsions made of a wide range of different fluids including non-volatile fluids or fluids that have a very low solubility in the outermost phase. Moreover, this device has the potential to reduce the shell thickness distribution of double emulsions produced through high throughput bulk emulsification methods because the shell thickness of the processed double emulsions is independent of that of injected double emulsions. The shell thickness of processed double emulsions only depends on the pressure profile in the device which can be controlled with the fluid flow rates and the viscosity of the oil. Therefore, this device offers new possibilities to fabricate capsules with thin shells whose thickness is well defined such that their stability and permeability can be closely controlled at high throughputs; this is of particular importance if capsules are used as delivery vehicles.

Acknowledgements

The authors would like to thank Gianluca Etienne for the synthesis of the surfactant. This work was financially supported by the Swiss National Science Foundation (SNSF, No. 200021_155997).

References

1 A. J. DeMello, *Nature*, 2006, **442**, 394–402.
2 R. Tomasi, J.-M. Noël, A. Zenati, S. Ristori, F. Rossi, V. Cabuil, F. Kanoufi and A. Abou-Hassan, *Chem. Sci.*, 2014, **5**, 1854–1859.
3 H. Song and R. F. Ismagilov, *J. Am. Chem. Soc.*, 2003, **125**, 14613–14619.
4 G. Amselem, C. Guermonprez, B. Drogue, S. Michelin and C. N. Baroud, *Lab Chip*, 2016.
5 F. Ma, M. Fischer, Y. Han, S. G. Withers, Y. Feng and G. Y. Yang, *Anal. Chem.*, 2016, **88**, 8587–8595.
6 H. F. Chan, S. Ma, J. Tian and K. W. Leong, *Nanoscale*, 2017, **9**, 3485–3495.
7 A. Zinchenko, S. R. A. Devenish, B. Kintses, P. Y. Colin, M. Fischlechner and F. Hollfelder, *Anal. Chem.*, 2014, **86**, 2526–2533.
8 A. G. Håti, T. Szymborski, M. Steinacher and E. Amstad, *Lab Chip*, 2018, **18**, 648–654.
9 M. B. Romanowsky, A. R. Abate, A. Rotem, C. Holtze and D. A. Weitz, *Lab Chip*, 2012, **12**, 802.
10 E. Amstad, M. Chemama, M. Eggersdorfer, L. R. Arriaga, M. P. Brenner and D. A. Weitz, *Lab Chip*, 2016, **16**, 138–155.

11 T. P. Lagus and J. F. Edd, *RSC Adv.*, 2013, **3**, 20512.
12 H. Zhang, G. Jenkins, Y. Zou, Z. Zhu and C. J. Yang, *Anal. Chem.*, 2012, **84**, 3599–3606.
13 W. Y. Zhang, W. Zhang, Z. Liu, C. Li, Z. Zhu and C. J. Yang, *Anal. Chem.*, 2012, **84**, 350–355.
14 E. Mastrobattista, V. Taly, E. Chanudet, P. Treacy, B. T. Kelly and A. D. Griffiths, *Chem. Biol.*, 2005, **12**, 1291–1300.
15 K. Bernath, M. Hai, E. Mastrobattista, A. D. Griffiths, S. Magdassi and D. S. Tawfik, *Anal. Biochem.*, 2004, **325**, 151–157.
16 A. Zinchenko, S. R. A. Devenish, B. Kintses, P. Colin, M. Fischlechner, F. Hollfelder, C. X. Zhao, D. Chen, Y. Hui, D. A. Weitz, A. P. J. J. Middelberg, A. Zacheo, A. Quarta, A. Zizzari, A. G. Monteduro, G. Maruccio, V. Arima, G. Gigli, C. X. Zhao, D. Chen, Y. Hui, D. A. Weitz, A. P. J. J. Middelberg, R. Zirbs, A. Lassenberger, I. Vonderhaid, S. Kurzhals and E. Reimhult, *ChemPhysChem*, 2015, **18**, 1393–1399.
17 S. W. Lim and A. R. Abate, *Lab Chip*, 2013, **13**, 4563.
18 S.-H. Kim, J. W. Kim, J.-C. Cho and D. A. Weitz, *Lab Chip*, 2017, **17**, 567–567.
19 C. X. Zhao, D. Chen, Y. Hui, D. A. Weitz and A. P. J. Middelberg, *ChemPhysChem*, 2017, **18**, 1393–1399.
20 C. Zhao, D. Chen, Y. Hui, D. A. Weitz and A. P. J. Middelberg, 2016, **2138**, 1553–1556.
21 S. S. Datta, A. Abbaspourrad, E. Amstad, J. Fan, S. H. Kim, M. Romanowsky, H. C. Shum, B. Sun, A. S. Utada, M. Windbergs, S. Zhou and D. a. Weitz, *Adv. Mater.*, 2014, **26**, 2205–2218.
22 a S. Utada, L. Chu, D. R. Link, C. Holtze and D. a Weitz, 2007, **32**, 702–708.
23 R. K. Shah, H. C. Shum, A. C. Rowat, D. Lee, J. J. Agresti, A. S. Utada, L. Y. Chu, J. W. Kim, A. Fernandez-Nieves, C. J. Martinez and D. A. Weitz, *Mater. Today*, 2008, **11**, 18–27.
24 E. Amstad, *Chim. Int. J. Chem.*, 2017, **71**, 334–341.
25 S.-H. Kim, J. W. Kim, J.-C. Cho and D. a Weitz, *Lab Chip*, 2011, **11**, 3162–3166.
26 H. C. Shum, J.-W. Kim and D. a Weitz, *J. Am. Chem. Soc.*, 2008, **130**, 9543–9.
27 H. C. Shum, D. Lee, I. Yoon, T. Kodger and D. A. Weitz, 2008, **24**, 7651–7653.
28 S. H. Kim, J. W. Kim, D. H. Kim, S. H. Han and D. A. Weitz, *Microfluid. Nanofluidics*, 2013, **14**, 509–514.
29 S.-H. Kim, J. Nam, J. W. Kim, D.-H. Kim, S.-H. Han and D. A. Weitz, *Lab Chip*, 2013, **13**, 1351.
30 S. H. Kim, H. C. Shum, J. W. Kim, J. C. Cho and D. A. Weitz, *J. Am. Chem. Soc.*, 2011, **133**, 15165–15171.
31 L. R. Arriaga, S. S. Datta, S. H. Kim, E. Amstad, T. E. Kodger, F. Monroy and D. a. Weitz, *Small*, 2014, **10**, 950–956.
32 L. R. Arriaga, E. Amstad and D. a. Weitz, *Lab Chip*, 2015.
33 A. Vian, V. Favrod and E. Amstad, *Microfluid. Nanofluidics*, 2016, **20**, 1–9.
34 Y. N. Xia and G. M. Whitesides, *Annu. Rev. Mater. Sci.*, 1998, **37**, 551–575.
35 J. C. Mcdonald, D. C. Duffy, J. R. Anderson and D. T. Chiu, 2000.
36 G. Etienne, M. Kessler and E. Amstad, *Macromol. Chem. Phys.*, 2017, **218**, 1–10.
37 C. Holtze, A. C. Rowat, J. J. Agresti, J. B. Hutchison, F. E. Angile, C. H. J. Schmitz, S. Koster, H. Duan, K. J. Humphry, R. A. Scanga, J. S. Johnson, D. Pisignano, D. a Weitz, F. E. Angilè, C. H. J. Schmitz, S. Köster, H. Duan, K. J. Humphry, R. A. Scanga, J. S. Johnson, D. Pisignano and D. a Weitz, *Lab Chip*, 2008, **8**, 1632–1639.
38 A. S. Chaurasia, D. N. Josephides and S. Sajjadi, *ChemPhysChem*, 2015, **16**, 403–411.
39 M. J. Hope, M. B. Bally, G. Webb and P. R. Cullis, *BBA - Biomembr.*, 1985, **812**, 55–65.
40 P. Sajeesh, M. Doble and a. K. Sen, *Biomicrofluidics*, 2014, **8**, 54112.